

Projection Effects on Physical Parameters Obtained from Solar Vector Magnetograms

Hui Li *

Purple Mountain Observatory, Chinese Academy of Sciences, Nanjing 210008
National Astronomical Observatories, Chinese Academy of Sciences, Beijing 100012

Received 2001 October 9; accepted 2001 December 3

Abstract Projection effects in Huairou solar vector magnetograms are corrected by transferring or mapping the observed vector magnetogram in the image plane to the heliographic plane (planar correction) and to the heliospheric coordinate system (spherical correction). The magnetograms after the correction are considerably different. The planar correction and the spherical correction lead to slightly different magnetic configurations, especially when the active region involved is far from the disk center. We also discuss the effects of the corrections on magnetic activity parameters, such as magnetic shear, current helicity, etc. It is shown that the neutral line is obviously distorted after the mapping. The mapping generally decreases the average shear angle on the neutral line by several degrees when the active region is in the eastern hemisphere, and increases it when in the western hemisphere. In most of the cases studied, the correction reduces the current helicity imbalance, and sometimes even changes its sign. It is found that the current helicity imbalance may change its sign in its evolution when there are apparent fluxes emerging from the lower photosphere. The corrections increase the noise level of B_z greatly, and decrease the noise level of B_t slightly. The accuracy of the magnetic field measurement at Huairou is estimated to be better than 20 G and 150 G for the longitudinal and the transverse component, respectively.

Key words: Sun: magnetic fields — Sun: activity — Sun: photosphere

1 INTRODUCTION

Magnetic field plays an important role in solar activity. The stressing and subsequent partial relaxation of magnetic fields in the active regions are generally accepted to be the energy source of solar flares. To quantitatively study the extent of stressed magnetic field as distinct from its potential field, Hagyard et al. (1984) defined a magnetic shear angle—the azimuth difference between the observed transverse magnetic field vector and the computed potential field vector that satisfies the boundary conditions imposed by the observed longitudinal field. In terms of

* E-mail: lihui@mail.pmo.ac.cn

the angular shear and other related parameters, such as weighted magnetic shear (Wang 1992) and shear index (Ambastha et al. 1993), quite a few authors have reported flare-related shear changes in recent years (e.g., Sakurai et al. 1992; Wang et al. 1994a; Chen et al. 1994; Ambastha et al. 1993; Wang et al. 1996a; Hagyard et al. 1999; Li et al. 2000a, 2000b). In addition to magnetic shear, current helicity has been extensively studied recently (e.g., Abramenko et al. 1997; Zhang & Bao 1998; Bao & Zhang 1998; Zhang & Bao 1999; Pevtsov et al. 2001; Zhang 2001). These works, most of which were done in the image plane, have revealed the relationship between the active-region magnetic fields and solar flares.

Correction for projection effects in solar vector magnetic field was demonstrated to be necessary in quantitative studies of related physical parameters, especially when the active region is far from the centre of the solar disk (Wilkinson et al. 1989; Venkatakrisnan et al. 1988, 1989, Gary & Hagyard 1990). Observationally, the measurement of the transverse field, both its magnitude and direction, is not as reliable as that of the longitudinal field (Gary et al. 1987). Transforming the magnetic field from the image plane to heliographic coordinates may introduce considerable inaccuracies into all components of the magnetic field (Wilkinson et al. 1989). Gary & Hagyard (1990) provided a full set of formulae needed to realize the mapping, and analyzed the magnetograms of NOAA 2684 and NOAA 4474 observed by the Vector Magnetograph at Marshall Space Flight Center. They pointed out that the neutral line is influenced by the off-center position of the active region, and full spherical geometry must be taken into account for off-center regions with central meridian distance (CMD) greater than 50° . Actually, at 23° heliocentric distance, spherical geometry already becomes apparent at the edge of the magnetogram when using planar approximation (Gary & Hagyard 1990). It was shown that the increased noise due to using the transverse field is tolerable for heliocentric distances less than 50° .

Wang et al. (1994b), in their study of NOAA 5747, transferred the vector magnetogram observed at Huairou from the image plane to the heliographic plane, but did not consider the curvature of the solar sphere. They found that the magnetic features after the correction are quite different from before, such as the shape of the neutral line, the characteristics of the emerging flux, the local area with high shear and the distribution of the shear angle near the neutral line. Moreover, because the transverse field was measured at the Fe I $\lambda 5324.19 \text{ \AA}$ line center at Huairou, we should pay attention to the magneto-optical effect as studied by Zhang (2000). He found that the Faraday effect is obvious when the magnetic field observation is made at a line center.

In this paper, we will map the observed vector magnetograms in the image plane to both the heliographic plane (planar correction) and the solar spherical coordinate system (spherical correction), and discuss the effects of these corrections on the magnetic configurations and physical parameters, such as the shear angle, current helicity, etc. We will briefly introduce the observation and calibration (Section 2), and describe the method of correction (Section 3). The influences of the corrections on the relevant physical parameters will be studied in Section 4, and conclusions and discussion are presented in Section 5.

2 OBSERVATION AND CALIBRATION

We choose the vector magnetic field data of six active regions (NOAA 8100, 8948, 9026, 9033, 9077 and 9087) to carry out the correction of the projection effects and study its impact

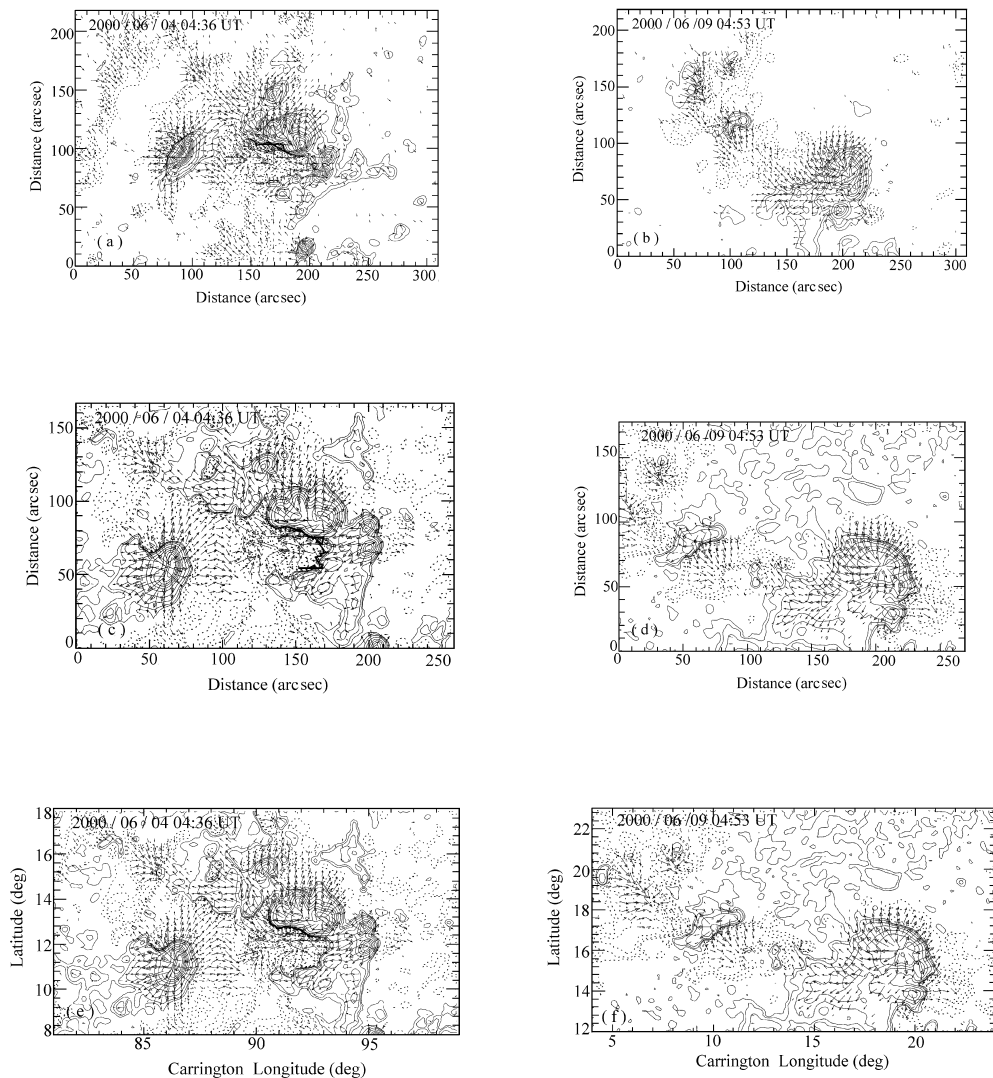


Fig. 1 Vector magnetograms of NOAA 9026 observed by the HVVM at 2000–06–04, 04:36 UT (left panel), (a) in the image plane, (c) after the planar correction, and (e) after the spherical correction for projection effect. The thick solid line marks the neutral line. (b), (d) and (f) on the right are the same as (a), (c) and (e) but for NOAA 9033 at 2000–06–09, 04:53 UT, and the neutral line is not shown. The center of the FOV is N12E29 for NOAA 9026 and N17E37 for NOAA 9033. North is on the top and west to the left. The contour levels for the longitudinal fields are $\pm 40, 80, 160, 320, 640, 960, 1280, 1600, 1920, 2240, 2560$ and 2880 G; solid contours for positive, and dotted contours for negative fields. This convention will be kept throughout this paper.

on the magnetic configurations and relevant physical parameters. All the magnetic field data used in this paper were observed under favorable seeing and weather conditions with the Huairou Video Vector Magnetograph (HVVM) mounted on the Solar Magnetic Field Telescope (SMFT) at Huairou Solar Observing Station (HSOS) of National Astronomical Observatories, Chinese Academy of Sciences (Ai & Hu 1986). The field-of-view (FOV) of the HVVM is about $320'' \times 220''$. The actual spatial resolution after a binning of 3×4 pixels is about $2'' \times 2''$. The vector magnetic fields were derived from the measurements of the four Stokes parameters I , Q , U , and V . The transverse field (parameters Q and U) was observed at the centre of the Fe I $\lambda 5324.19 \text{ \AA}$ line, and the longitudinal field (parameter V), at 0.075 \AA from the line center.

The calibration of the Huairou Vector Magnetograph has been discussed by Ai et al. (1982), Wang et al. (1996a, 1996b). The noise level of the original magnetograms is usually less than 20 G for the longitudinal component and about 100 G for the transverse one (see below). We use the square-root method to calibrate the transverse field (Eq.(1)). Specifically, for the HVVM data (Wang et al. 1996b),

$$B_t = 9.37 \times 10^3 \times (Q^2 + U^2)^{1/4} \text{ G.} \tag{1}$$

The direction of the transverse field is determined and the ambiguity of the B_t direction is resolved before making any quantitative calculation (Wang et al. 1994b).

3 CORRECTION FOR THE PROJECTION EFFECTS

To study the impact of the planar and spherical corrections of the projection effects on the magnetic structures, features, and the relevant parameters, we use the formulae given by Gary and Hagyard (1990) to make both the planar and spherical mappings of the observed vector magnetograms in the image plane. After the correction, we only save the data of a rectangle, in which all points have valid values of B_z and B_t , by symmetrically discarding the boundary rows and columns. This makes the location of the center of resultant magnetogram on the solar disk almost unchanged compared with the original one. We calculate the 3σ noise level for each magnetogram in a small area that contains the weakest field of the whole field.

Figure 1 shows the vector magnetograms in the image plane of NOAA 9026 at 2000-06-04, 04:36 UT (Figure 1a) and of NOAA 9033 at 2000-06-09, 04:53 UT (Figure 1b). The center of the FOV is N12E29 for NOAA 9026 and N17E37 for NOAA 9033. The magnetograms corrected for the projection effects are also displayed in Figure 1. The neutral line of NOAA 9026 is shown thick.

From the figure we notice that, after the mapping, the shape of the neutral line changed obviously and the average shear angle decreased (Table 1). The longitudinal component was affected more than the transverse component by the corrections due to the mismatch of their measurement accuracy. The increased noise is still tolerable when the CMD of the active region is 37° , although there are some extra magnetic features, such as small positive and negative magnetic islands on the corrected magnetograms. The mapping also leads to different magnetic structures and configurations. For example, the positive magnetic island in the upper-left quarter is apparently larger in Figure 1b than in the corrected magnetograms of Figures 1d and 1f. By carefully comparing Figure 1c with Figure 1e and Figure 1d with Figure 1f, we find that the planar and spherical corrections result in slightly different magnetograms, especially near the edge of the FOV. Furthermore, the neutral lines, the average shear angles on the neutral lines and the current helicity imbalance corresponding to the two mappings also have some differences (Tables 1 and 2).

In addition to the magnetograms shown above, we investigated magnetograms of some other active regions including NOAA 8100, 8948, 9077 and 9087 to study the noise resulting from the mappings. We consider the change in the 3σ noise level before and after the corrections as a function of the distance of the active region from the disk center. The results are plotted in Figure 2.

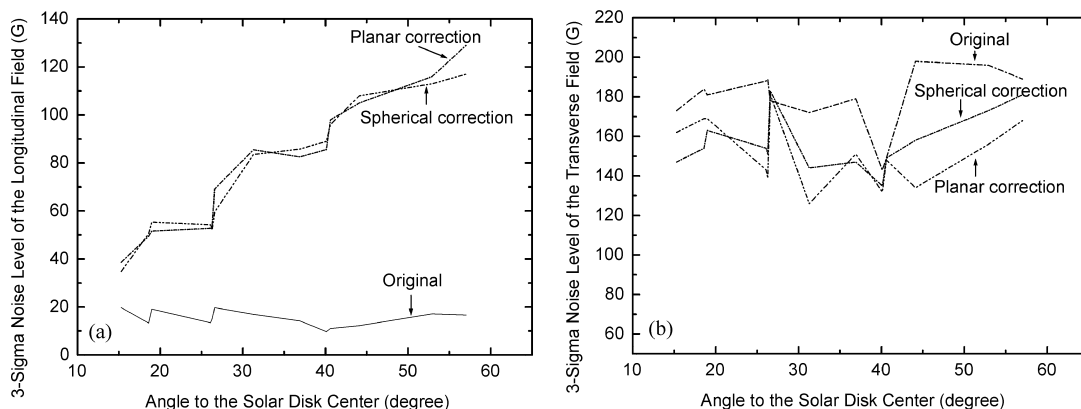


Fig. 2 Variation of the 3σ noise level with the distance of the active region to the disk center for (a) the longitudinal field and (b) the transverse field. The methods of calibration and correction are indicated in the figure beside each plot.

From Figures 1–2, we see that the mappings lead to significantly higher noise levels. The mappings increased the noise level of B_z greatly. The noise level of B_z after the corrections is between about 60 G to more than 100 G for regions with CMDs less than 37° . In contrast, the noise level of B_t after the corrections of projection effects decreased slightly. Therefore, for the vector magnetograms observed at Huairou, the noise caused by the correction of the projection effects is tolerable when the CMD of the active region is less than 37° .

If we take the 3σ noise level as an indicator of the field measurement accuracy, then from Figure 2 we have that the measuring accuracy of B_z is about 16 G in the image plane, and that of B_t is about 180 G. We will discuss this point further in Section 5.

Table 1 Effect of Corrections of Projection Effects on the Average Shear Angle

Date (yyyy mm dd)	Time (UT)	AR Number	FOV Center	Average Shear Angle (deg.)		
				Original	Planar	Spherical
2000-07-12	03:33	9077	N10E26	38.9	32.2	34.8
2000-07-15	00:53	9077	N10W14	32.3	39.3	41.5
2000-06-10	04:47	9033	N17E24	18.8	30.1	25.4
2000-06-12	04:24	9033	N17W05	40.7	41.6	41.1
2000-06-04	04:36	9026	N12E29	48.2	34.1	34.2
2000-06-07	07:34	9026	N12W15	32.3	38.9	41.8
2000-04-09	05:10	8948	S14E10	49.2	44.7	44.9
2000-04-11	00:01	8948	S14W13	45.7	50.6	55.4
1997-10-31	03:57	8100	S13E20	47.2	44.0	44.9
1997-11-03	02:48	8100	S13W20	49.2	52.0	56.1

4 EFFECT OF THE CORRECTIONS ON PHYSICAL PARAMETERS

4.1 Effect on Magnetic Shear

We cited the definition in Hagyard et al. (1984) for the magnetic shear angle in our study (Section 1). The ambiguity of the transverse field direction has been resolved. We only consider those points with $B_t > 150$ G, considering the low accuracy in the measurement of the transverse fields. The average shear angles ($\bar{\varphi} = \Sigma|\varphi|/n$) along the neutral line of the selected active regions are computed. The results are presented in Table 1.

If we only consider photon statistical noise and take the measuring accuracy of B_t to be 150 G, the uncertainty in the value of the shear angle, which depends on the transverse field strength, is about 0.90° when the transverse field is 300 G and 0.12° when the transverse field is 500 G. The average shear angle will have errors smaller than these by a factor of $1/\sqrt{N}$ (N = number of data points). Errors may also arise if the resolution of the azimuth ambiguity is not correctly made. However, these errors are difficult to quantify. The active regions listed in Table 1 are large and have a strong transverse field along the neutral line (most of them have average B_t greater than 800 G on the neutral line). Therefore, the inaccuracy of the average shear angle in Table 1 is very small and we did not place an error bar there.

It can be seen from Table 1 that the corrections change the average shear angle on the neutral line by $3\text{--}10^\circ$. Meanwhile, in most of the cases studied, the corrections tend to decrease the average shear angle for active regions located in the eastern hemisphere, and increase the average shear angle for those in the western hemisphere (Table 1).

4.2 Effect on Current Helicity

The current helicity is defined as

$$h_c = B_z \cdot \left(\frac{\partial B_y}{\partial x} - \frac{\partial B_x}{\partial y} \right), \tag{2}$$

where B_z is the longitudinal component of the magnetic field. We compute the current helicity imbalance $\rho_c = \frac{\Sigma h_c}{\Sigma |h_c|} \times 100\%$ given by Bao and Zhang (1998) for the active regions considered in this paper to study the impact of the projection effects on the current helicity. The noise level of the current J_z in our calculation is about 0.001 A m^{-2} when taking the noise levels of B_z and B_t to be 20 G and 100 G, respectively (Bao & Zhang 1998). Therefore, we only check the current helicity for those points where $B_z > 20$ G, $B_t > 100$ G and $J_z > 0.001 \text{ A m}^{-2}$. The calculated values of the relevant parameters are listed in Table 2.

Table 2 shows that the corrections can significantly change the current helicity imbalance ρ_c and sometimes may even change the sign of ρ_c (e.g., the case of NOAA 9033 on 2000–06–10 in Table 2). There is another point that is worth mentioning, i.e., the sign of the current helicity imbalance of an active region may change either from positive to negative (e.g., NOAA 8100), or from negative to positive (e.g., NOAA 9026). On examining the evolution of the two active regions (Figure 3), we notice that there were obvious fluxes emerging from the lower photosphere on the days when the current helicity imbalance reversed its sign. It is quite possible that the emerging flux is responsible for the sign reversal.

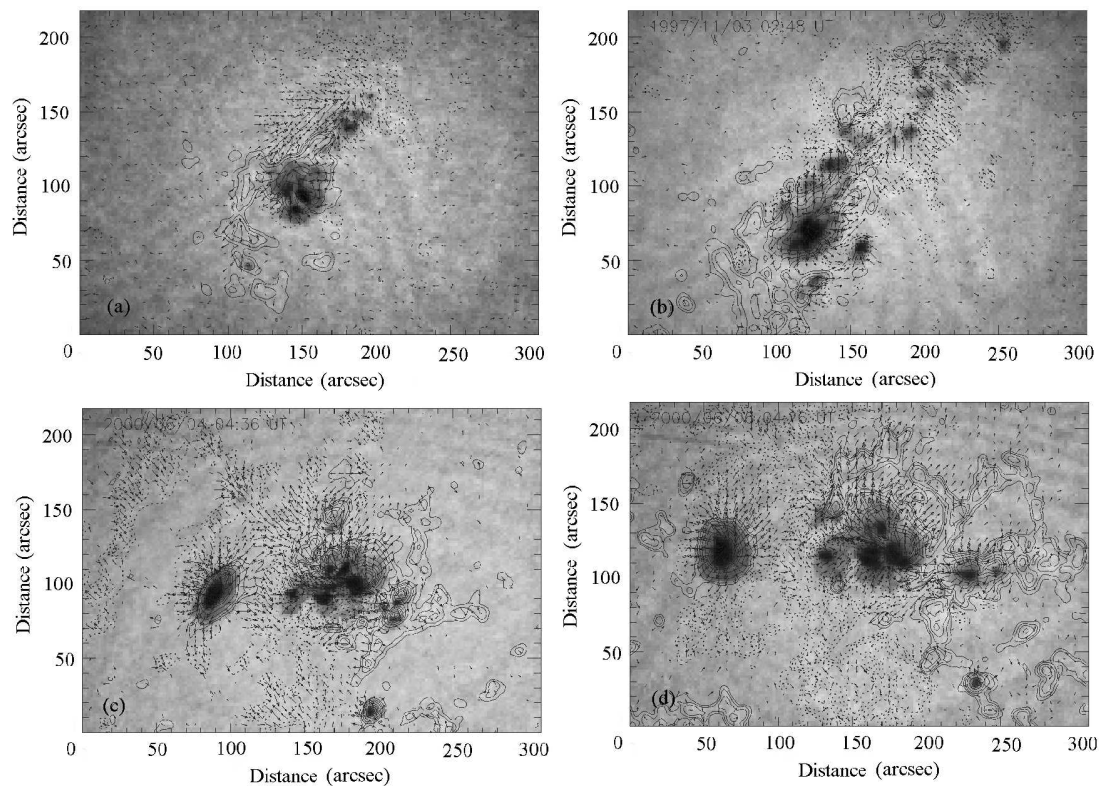


Fig. 3 Vector magnetograms of NOAA 8100 at 1997–10–31, 03:09 UT (a), and 1997–11–03, 02:48 UT (b), and of NOAA 9026 at 2000–06–04, 04:36 UT (c) and 2000–06–06, 04:26 UT (d). Same contour convention as Figure 1. The background is the photospheric image of the corresponding active region showing the sunspots.

5 CONCLUSIONS AND DISCUSSION

We studied the corrections of projection effects in solar vector magnetograms observed by the HVVM at HSOS, National Astronomical Observatories, Chinese Academy of Sciences, and its effects on the magnetic configurations and features of the active regions and the relevant physical parameters, such as the magnetic shear angle and current helicity imbalance. It is shown that, in addition to the magneto-optical effect (Zhang 2000), we should also pay attention to the projection effects in quantitative analysis of the HVVM vector magnetic field data, especially when the active region is located far from the centre of the solar disk.

The mapping of the vector magnetograms from the image plane to the heliographic plane and the spherical coordinate system considerably changes the shape and position of the neutral line (Wilkinson et al. 1989, Wang et al. 1994b), the length of neutral lines with strong shear (Venkatakrisnan et al. 1988), and consequently the distribution of the shear angle and the average shear angle along the neutral line, and even though the projection effects did not significantly affect the critical shear, the number of ‘critically sheared’ pixels may change

(Venkatakrishnan et al. 1989). The change of the average shear angle amounts to several degrees in the cases studied here, which needs to be taken into account when studying the change of the shear angle in the evolution of the active region and in a flaring process. This effect has not been mentioned in previous works (e.g., Li et al. 2000a, 2000b, Chen et al. 1994, Wang et al. 1994a). We found in our cases that, after the correction the average shear angle tends to decrease when the active region is located in the eastern hemisphere and to increase when in the western hemisphere. Possibly this is because the shift in the Fe I $\lambda 5324.19 \text{ \AA}$ line due to the rotation of the Sun leads to that the magnetic field is measured at different wavelengths for the eastern and western hemispheres.

The corrections induce extra noise and magnetic structures (see Figure 1). In our cases, the noise levels of B_z and B_t in the original magnetograms are about 16 G and 180 G, respectively. Here, we take the 3σ noise level in a selected small area in the FOV where the magnetic field is the weakest for the whole region, as the measuring accuracy. Actually, the field could not be exactly zero even in the weakest area, thus the 3σ level comprises the measuring accuracy and the fluctuation of some weak field. In other words, the real measuring accuracy is better than the 3σ noise level. Therefore, we may conclude that the measuring accuracy of B_z and B_t of HSOS observation are better than 20 G and 150 G, respectively.

Table 2 Effect of Correction of Projection Effects on the Current Helicity Imbalance

Date (yyyy mm dd)	Time (UT)	AR Number	FOV Center	Current Helicity Imbalance (%)		
				Original	Planar	Spherical
2000-07-12	03:33	9077	N10E26	-14.7	-13.3	-13.5
2000-07-15	00:53	9077	N10W14	-4.0	-3.9	-3.4
2000-06-10	04:47	9033	N17E24	0.52	-0.25	-3.4
2000-06-12	04:24	9033	N17W05	-4.9	-8.2	-5.1
2000-06-04	04:36	9026	N12E29	-28.4	-19.5	-17.8
2000-06-04	23:56	9026	N12E17	-4.78	-2.35	-2.10
2000-06-06	04:26	9026	N12E02	6.80	0.88	1.05
2000-06-07	07:34	9026	N12W14	22.4	15.4	12.9
2000-04-09	05:10	8948	S14E10	13.3	13.9	14.6
2000-04-11	00:01	8948	S14W13	-14.1	-12.0	-13.9
1997-10-31	03:57	8100	S13E20	21.8	7.38	9.60
1997-11-01	02:08	8100	S13W06	-3.20	-7.15	-6.11
1997-11-03	02:48	8100	S13W20	-15.7	-0.72	-1.80

The corrections may increase the noise level of B_z to about 60–100 G. And the resultant extra noise increases with the CMD of the active region. In contrast, the noise of B_t was slightly decreased after the mappings. This could be explained by the mismatch of the measuring accuracies of B_z and B_t . Because the measuring accuracy of B_t is much lower than that of B_z , it results in much more noise in B_z after the correction than what B_z causes in B_t . It is shown above that the increased noise and the impact of the corrections on the magnetic features and configurations are tolerable when the CMD of the active region is less than 37° .

The mapping of the vector magnetograms also affects the current helicity. The current helicity imbalance (Bao & Zhang 1998) decreased in most of the cases studied (Table 2). It was found that the current helicity imbalance of an active region may change its sign during the evolution of the active region (Table 2). The emerging flux in active regions may be responsible

for such change. As new flux emerges, new current system may be formed, which interacts with the existing current system and subsequently power and trigger a solar flare (Wang et al. 1994b). If the emerging flux has a strong helicity with opposite sign to the pre-existing one, it may overcome the latter and change its sign when the new flux collides with the old.

The planar and spherical corrections have somewhat different effects on the neutral line, the shear distribution, the average shear angle, and the current helicity imbalance (Figure 1, Tables 1 and 2), even though the difference is not significant. Even on magnetograms with a CMD of 29° the difference is discernible (Figure 1), especially for the points near the edge of the FOV (Gary & Hagyard 1990). Therefore, for more accurate study in the future, the spherical correction is recommended.

Acknowledgements The author thanks Professor H.Q. Zhang for his valuable comments on the manuscript and inspiring discussion. This work was supported by the National Natural Science Foundation of China (NSFC, 49990451) and the National Basic Research Priorities Project (G2000078402).

References

- Ai G. X., Hu Y. F., 1986, *Publ. Beijing Astron. Obs.*, 8, 1
 Ai G. X., Li W., Zhang H. Q., 1982, *Chin. Astron. Astrophys.*, 6, 129
 Ambastha A., Hagyard M. J., West E. A., 1993, *Solar Phys.*, 148, 277
 Abramenko V. I., Wang T., Yurchishin V. B., 1997, *Solar Phys.*, 174, 291
 Bao S. D., Zhang H. Q., 1998, *ApJ*, 496, L43
 Chen J. M., Wang H. M., Zirin H. et al., 1994, *Solar Phys.*, 154, 263
 Gary G. A., Moore R. L., Hagyard M. J. et al., 1987, *ApJ*, 314, 782
 Gary G. A., Hagyard M. J., 1990, *Solar Phys.*, 126, 21
 Hagyard M. J., Smith J. B. Jr., Teuber D. et al., 1984, *Solar Phys.*, 91, 115
 Hagyard M. J., Stark B. A., Venkatakrisnan P., 1999, *Solar Phys.*, 184, 133
 Li H., Sakurai T., Ichimoto K. et al., 2000a, *PASJ*, 52, 465
 Li H., Sakurai T., Ichimoto K. et al., 2000b, *PASJ*, 52, 483
 Pevtsov A. A., Canfield R. C., Latushko S. M., 2001, *ApJ*, 549, L261
 Sakurai T. et al. 1992, *PASJ*, 44, L123
 Venkatakrisnan P., Hagyard M. J., Hathaway D. H., 1988, *Solar Phys.*, 115, 125
 Venkatakrisnan P., Hagyard M. J., Hathaway D. H., 1989, *Solar Phys.*, 122, 215
 Wang H. M., 1992, *Solar Phys.*, 140, 85
 Wang H. M., Ewell Jr. M. W., Zirin H. et al., 1994a, *ApJ*, 424, 436
 Wang T. J., Xu A. A., Zhang H. Q., 1994b, *Solar Phys.*, 155, 99
 Wang J. X., Shi Z. X., Wang H. N. et al., 1996a, *ApJ*, 456, 861
 Wang T. J., Ai G. X., Deng Y. Y., 1996b, *Astrophyscis Reports, Publ. Beijing Astron. Obs.*, 28, 31
 Wilkinson L. K., Emslie A. G., Gary G. A., 1989, *Solar Phys.*, 119, 77
 Zhang H. Q., 2000, *Solar Phys.*, 197, 235
 Zhang H. Q., 2001, *ApJ*, 557, L71
 Zhang H. Q., Bao S. D., 1998, *A&A*, 339, 880
 Zhang H. Q., Bao S. D., 1999, *ApJ*, 519, 876